Colloids and Surfaces B: Biointerfaces 159 (2017) 97–107

Contents lists available at ScienceDirect

Colloids and Surfaces B: Biointerfaces

journal homepage: www.elsevier.com/locate/colsurfb

Full Length Article

# Investigating *the race for the surface* and skin integration in clinically retrieved abutments with two-photon microscopy

D. Kapsokalyvas[a,1], M. van Hoof[b,*,1], S. Wigren[c], T. Chimhanda[a], H.J. Kuijpers[a], F.C.S. Ramaekers[d], R.J. Stokroos[b], M.A.M.J. van Zandvoort[a]

[a] *Department of Molecular Cell Biology, CARIM School for Cardiovascular diseases, Maastricht University Medical Center, UNS 50, 6229 ER Maastricht, The Netherlands*
[b] *Department of Otorhinolaryngology and Head and Neck Surgery, Maastricht University Medical Center, PO Box 5800, 6202, AZ, Maastricht, The Netherlands*
[c] *Cochlear Bone Anchored Solutions, AB, Mölnlycke, Sweden*
[d] *Department of Molecular Cell Biology, GROW-School for Oncology and Developmental Biology, Maastricht University Medical Center, PO Box 616, 6200 MD Maastricht, The Netherlands*

ARTICLE INFO

*Article history:*
Received 3 April 2017
Received in revised form 14 July 2017
Accepted 26 July 2017
Available online 27 July 2017

*Keywords:*
Hydroxyapatite
Two-photon microscopy
Skin integration
Abutment

ABSTRACT

Bone conduction hearing implants can rehabilitate some types of hearing loss. A hydroxyapatite (HA)-coated skin-penetrating abutment was developed to allow for soft tissue preservation and increased skin-abutment adherence. Inflammation is thought to relate to bacterial infection of pockets around the abutment. Upon integration, the host's ability to cover the abutment surface ("race for the surface"), and thus control and prevent competitive bacteria from colonizing it, is improved. However, the attachment mechanisms behind it are not clear. In this study, we applied two-photon microscopy to visualize tissue attachment on abutments retrieved from patients. Skin integration markers were validated and applied to four HA-coated abutments. Evidence of skin integration was found, including the presence of hemidesmosomes, a basement membrane, dermal collagen and vascularization. Cases with clinical signs of severe inflammation and evident biofilm formation showed limited skin integration based on these indicators, confirming the applicability of the "race for the surface" model.



## 1. Introduction

Percutaneous implants are associated with frequent inflammation throughout all branches of medicine [1,2]. Any implant that breaches the barrier of the skin, subjects its host to increased influence of the external environment [3]. A point of entry for pathogens is created, challenging the host's immune defense [4,5] and wound healing response [6]. In this respect, the semi-implantable bone conduction hearing implant (BCHI) is no exception [7]. The implant system consists of a screw-shaped intraosseous implant that integrates with the skull bone (osseointegration [8]) and an abutment that permanently penetrates the skin and attaches to an external sound processor. This system rehabilitates patients with a specific type of hearing impairment [9]. However, inflammation of the tissue surrounding the skin-penetrating abutment affects approximately 30% of patients within two years [10].

Conventionally, percutaneous BCHIs were placed using extensive soft tissue reduction around the all-titanium abutment to minimize the amount of inflammation by stabilizing the skin [7] and preventing deep peri-abutment skin pockets to form. However, the removal of subcutaneous tissues is associated with other complications, such as numbness and cosmetic issues [11]. A hydroxyapatite(HA)-coated titanium abutment was developed to mitigate the need for soft tissue reduction [12]. Previous investigations have shown that, in contrast to the traditional titanium abutments, HA allows attachment of tissue from the host [13]. A tight dermal adherence has been demonstrated in animal models [12,14]. A tight seal between the abutment surface and adjacent soft tissues [15,16] prevents bacteria from accumulating at the skin-abutment interface ('*pocket formation*'). As a result, bacteria are inhibited from colonizing the abutment surface before the host integrates with it (a model referred to as the '*race for the surface*' [17]). If the host is successful in forming a structural connection with the abutment, this mechanical barrier in association with its immune response may protect the abutment surface from continuous attempts of invasion by bacteria [13].

* Corresponding author.
*E-mail address:* marc.hoofvan@mumc.nl (M. van Hoof).
[1] *These authors have contributed equally to this investigation.

http://dx.doi.org/10.1016/j.colsurfb.2017.07.072

The competition between nutrient driven bacteria and the host's cells to populate a surface is complex and dynamic [18]. Both modify their behavior in response to the actual situation (e.g. available nutrients vs. breach of integrity of the host) and each other (e.g. infection, evasion [19,20], bacterial tolerance of the host [20,21], tolerance to antibiotic treatment [22] or eradication). Both also change their behavior over time (e.g. biofilm formation vs. different phases of the immune response, wound closure and a foreign body reaction [23]). The host response includes many different solitary and collaborating cell types which are either blood-borne (e.g. neutrophils, macrophages, fibrocytes [24]) or locally present in the skin [4] (e.g. keratinocytes, corneocytes, fibroblasts and dendritic cells). The balance is further complicated by bacterial colonies that can be composed of multiple species with different degrees of virulence and different modes of action (e.g. intracellular infection) [2].

The dynamics between bacteria and the host cells, which influences the "*race for the surface*", is often investigated in a simplified manner using a combination of cell line(s) and selected bacterial species *in vitro* [25]. As long as the complexity of the process is not sufficiently reflected in these experiments, the ability to translate in vitro research to clinical practice is restricted. To date, no artificial implant has achieved an incidence of inflammation as low as physiological, soft tissue penetrating systems. Importantly, the challenge of a successful abutment-skin interface does not only lie in creating a mechanical seal or achieving integration, but also in reestablishing such an interface over a lifetime (e.g. in response to infections, skin tearing, abutment changes etc.). Percutaneous abutments retrieved from patients, in contrast to common animal models, represent the actual, prevalent states in which they can be found in daily clinical practice. The multitude of known and unknown variables [6] that influence the skin-abutment interface converge to and determine these clinical states (e.g. skin integration, fibrotic encapsulation, bacterial colonization, etc.). Therefore, one of the objectives of this *ex vivo* clinical investigation was to assess the feasibility to study the skin-abutment interface in high detail in devices that have been in situ.

In a previous scanning electron microscopy (SEM) study [13], it was shown that HA-coating of an abutment results in almost full tissue coverage with an arrangement that suggests direct attachment. However, SEM did not allow to specifically analyze the cellular attachment components in the abutment-tissue interface, and therefore elucidating the mechanisms of attachment was not possible. Conventional histopathologic sample preparation and examination is complicated because of the hardness of titanium, which commonly complicates producing thin enough sections for proper subcellular resolution. While methods exist to produce thin sections, the required use of embedding materials restricts the choice of stains. By using such an approach in an animal study Larsson et al. [12] reported dermal adherence to the HA-coated abutments, limited pocket formation and epidermal downgrowth as compared to all-titanium abutments, showing a proof of concept of skin integration of HA-coated abutments.

The method proposed here combines two-photon laser scanning microscopy (TPM) with a specific set of markers to represent skin integration and 3D imaging methodology to analyze the full-length of the abutment-tissue interface. TPM has been applied successfully in imaging human skin ex vivo [26] and in vivo [27–30]. It features the advantage of cross-sectional deep tissue penetration without destructive sectioning. Cellular and connective tissue morphology can be locally visualized with high contrast, even without labeling [31]. Using TPM we aimed at visualizing the structures that can adhere to the HA surface. We hypothesize that hemidesmosome complexes relevant for cell-substratum adhesion [32] and the creation of a basement membrane are the mechanisms that are used by basal keratinocytes, possibly in conjunction with other cells, to attach to the surface of an HA-coated abutment. To visualize epidermal attachment, integrin-α6 was labelled, a protein complex used by basal cells to form hemidesmosomes which connect the epidermis to the basement membranes [33]. Collagen IV is expressed in the basement membranes of the skin that interconnects the epidermis to the dermis. Collagen IV is also found in basement membrane of vasculature [34] and skin appendages [35]. Visualization of dermal collagen was pursued using CNA35 (collagen adhesion protein 35), which is known to bind strongly to various collagen types, among which collagen I, III and IV [36,37]. Cell nuclei were stained using DAPI fluorescent stain, and the morphology of the nucleus was used as an indication of the cell type. Bacterial DNA can also be stained by DAPI, thus allowing the identification of biofilm on the abutment surface.

The objective of this investigation was to develop and validate the proposed methodology and investigate molecular aspects of skin integration in relation to '*the race for the surface model*' in abutments retrieved in clinical practice.

## 2. Materials and methods

### 2.1. Ethics

The procedures in this investigation were in accordance with the legislation and ethical standards on human experimentation in the Netherlands. The Dutch national competent authority, Centrale Commissie Mensgebonden Onderzoek (CCMO), was consulted about the obligation of formal competent authority and ethical approval. No formal approval was required as the study procedures were considered to be within the law (Wet op Mensgebonden Onderzoek). The anonymized materials studied were derived from patients and classified as surgical by-products. No patient identifying information was retained and samples were coded for handling. Verbal informed consent was obtained prior to removal of the sample for the specific aim. All samples were collected and analyzed at the Maastricht University Medical Center.

### 2.2. Sample collection

For the purpose of validating the method, reference skin biopsies using a 1 mm biopsy punch (Miltex inc., York, USA) were collected from retro-auricular skin removed during implant surgery in a patient receiving a BCHI. The surgical procedure involves punching a 5 mm hole through the full-thickness skin at the implant site, approximately 5 cm above and behind the ear, hence leaving the punch content as a waist product from which control biopsy samples were collected. The biopsy thickness (1 mm) is comparable to the thickness of the tissue that can remain on the abutment after extraction. Biopsies were immediately placed in fixation medium.

One all-titanium (Fig. 1A) Cochlear™ Baha® Abutment (Cochlear Bone Anchored Solutions AB, Mölnlycke, Sweden) and four HA-coated Cochlear Baha BA400 Abutments (top diameter 7.3 mm, bottom diameter 4.0 mm, Fig. 1B) were collected from patients scheduled for abutment change or removal. The abutments were removed by unscrewing them from the osseointegrated implant and pulling the abutment out of the skin. Demographics and clinical history were collected and all information relating to the patient was anonymized. The abutments were immediately immersed in fixation solution.

All clinical samples (abutments and biopsies) were fixed in 3.7% formaldehyde in phosphate buffered saline pH 7.4 (PBS) for 15 min, and stored in PBS with 15 mM sodium azide at 4 °C. One unused Cochlear Baha BA400 Abutment, taken directly from the sterile packaging, served as a reference sample for the HA autofluorescence signal.

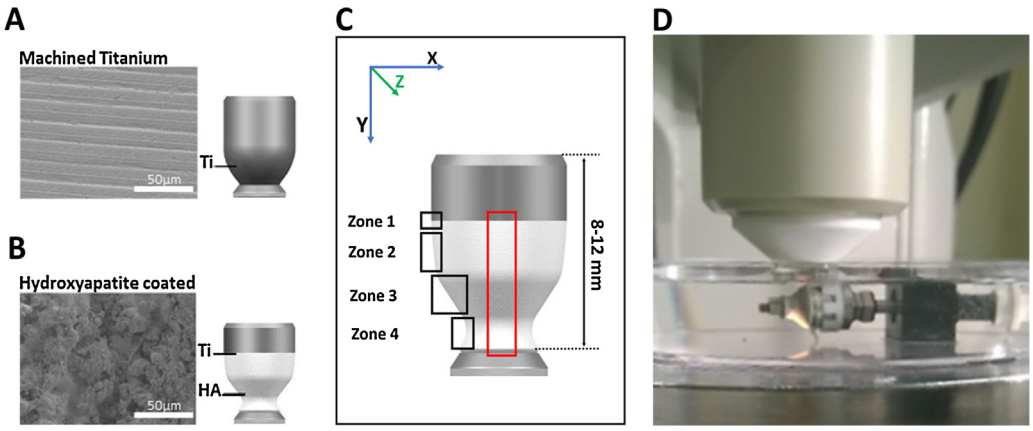


**Fig. 1.** Overview of abutments and the abutment rotation mount.(For interpretation of the references to colour in this figure legend, the reader is referred to the web version of this article.)
**A)** Conventional medical grade titanium (Ti) abutment with a smooth surface as shown in the scanning electron micrograph. **B)** Hydroxyapatite (HA, in white) coated abutment. The scanning electron micrograph shows the rough surface. **C)** HA coated abutment dimensions. Zones 1–4 are depicted using black rectangles. Red rectangle indicates the longitudinal stripe imaged in Figs. 4G and 7G. On top left, the coordinate system is indicated. Imaging direction is from top to bottom. **D)** The abutment rotation mount used in the two-photon microscope was made using common components (Cochlear™ abutment inserter and LEGO® parts) and allows for non-destructive scanning of the entire abutment surface.

In order to standardize the imaging procedure (see below) and to enable inter-abutment comparison, the abutments were divided into zones of interest as seen in Fig. 1B. The HA coating covers most of the abutment length starting from the base. The upper titanium part of this abutment, which is intended to protrude above skin level, is not coated. Zone 1 is the region where the HA coating ends and the titanium surface starts. When in situ, this zone corresponds approximately with the level of the stratum corneum of the patient's skin. Zone 2 includes the cylindrical HA-coated region of the top part of the abutment. Zone 3 includes the converging part of the abutment and Zone 4 the concave part at the bottom of the abutment that meets the osseointegrated implant.

### 2.3. Fluorescent labeling

Samples (abutments and biopsies) were washed thrice for 10 min with PBS on an oscillating platform and were permeabilized with 0.1% Triton-X 100 for 15 min at room temperature (RT). After washing with PBS, samples were incubated with the primary antibodies. These included mouse anti-integrin-α6 (ab20142, Abcam, Cambridge, UK) using a 1:100 dilution and rabbit anti-human collagen IV [38] using a 1:1000 dilution in PBS containing 1% bovine serum albumin (BSA) for 1 h at RT. After washing thrice with PBS for 10 min, secondary antibodies AF568 conjugated goat anti-mouse (ab1754731, Abcam, Cambridge, UK) and AF488 conjugated goat anti-rabbit (ab150077, Abcam, Cambridge, UK), each in a 1:500 dilution in PBS containing 1% BSA, were applied to the samples for 1 h at RT, followed by a washing step. For staining of dermal collagen, collagen-binding adhesion protein 35 (CNA35) [37], conjugated with OG488 or AF568 was used for 1 h incubation (0.5 μM) at RT. Afterwards, samples were washed thrice for 10 min with PBS on an orbital shaker. All samples were stained for DNA with 4′,6-Diamidino-2-Phenylindole (DAPI, Roche Diagnostics B.V., Almere, Netherlands) using a dilution of 0.5 μg/ml in PBS. Samples were stored in PBS with 15 mM sodium azide at 4 °C until the imaging session. Table 1 shows the fluorescent stains used for each sample.

### 2.4. Two-photon microscopy and image analysis

For imaging, a Leica TCS SP5 (Leica Microsystems GmbH, Wetzlar, Germany) two-photon laser scanning microscope was used with a Ti-Sapphire Chameleon Ultra II (Coherent Inc, Santa Clara, CA,USA) laser. Excitation was at 820 nm, except for Case 4 were excitation was at 780 nm. A Leica objective, HCX APO L 20x/1.00 was used. Fluorescence detection was performed using three detectors set according to the emission spectra of the dyes used in each sample (Table 1). Image acquisition was performed simultaneously for all channels. DAPI was detected at 430–490 nm, AF488 at 510–550 nm, AF568 at 595–640 nm, CNA/OG488 at 510–550 nm and CNA/AF568 at 595–640 nm. Second harmonic generated signal (SHG) from dermal collagen, was detected with a forward detector with a bandpass filter (380–420 nm).

The biopsy samples were mounted for imaging inside a 50 mm Petri dish filled with PBS and immobilized with agarose gel. Abutment samples were attached to an Abutment inserter (Cochlear Bone Anchored Solutions AB, Mölnlycke, Sweden) and mounted on a custom made rotation mount inside a 50 mm Petri dish filled with PBS (Fig. 1D). This allowed 360° rotation around the medial axis, enabling visualization of the total abutment surface.

Noise was removed from all images using a non-linear filter (Guidedfilter) in Mathematica (Wolfram Research, Inc., Mathematica, Version 10.4, Champaign, IL, USA). For the 3D reconstruction of the extended field of view (full-length abutment) of the HA-coated abutments, a series of consecutive z-stacks, covering the entire surface from top to the bottom, were acquired. These z-stacks were subsequently stitched using the Pairwise stitching [40] plugin of ImageJ. The stitched z-stack was used to make the 3D reconstruction. Each z-stack was acquired with a 2.5 μm step size, except for one case where a 5 μm step size was used. In order to visualize the full view of the abutments in one image, a maximum projection image was created from the stitched z-stacks. This produced the longitudinal stripes presented in Figs. 4G, 7G, and 9. All abutment images and image projections are in the XY plane as indicated in Fig. 1C. Imaging direction is always from the top to the bottom of the abutment. Images were processed and analyzed using Fiji ImageJ [41].

## 3. Results

### 3.1. Sample inclusion and patient demographics

Patient demographics and their clinical history are presented in Table 1. Biopsy samples were collected from one patient during BHCI placement (Control 1). Abutments were retrieved from five patients (four patients with a HA-coated abutment and one patient with an all-titanium abutment). At the time of removal, all abut-

**Table 1**
Demographics data and (immunofluorescent) stains used.

| Sample | Case # (Abutment length) | Age/sex | Relevant history | In situ period | Removal indication | Inflammation | Soft tissue level | Stains |
|---|---|---|---|---|---|---|---|---|
| Skin Biopsies | | 44/F | – | | Waist product BCHI surgery | No | | DAPI Collagen IV (488) Integrin-α6 (568) |
| Titanium abutment | | 72/F | – | 14 years | Abutment change | | Over the top of the abutment | No (autofluorescence) |
| HA-coated abutments | Case 1 (8 mm) | 26/F | – | 2 years | Recurrent minor inflammation | Minor | High level of soft tissue | DAPI Collagen IV (488) Integrin-α6 (568) |
| | Case 2 (12 mm) | 60/F | Cogan Syndrome | 2.5 years | Severe inflammation | Severe | Normal level of soft tissue | DAPI CNA35 (488) |
| | Case 3 (10 mm) | 56/M | – | 2 years | Skin overgrowth | Moderate | Over the top of the abutment | DAPI Collagen IV (488) Integrin-α6 (568) |
| | Case 4 (10 mm) | 60/F | – | 1.5 years | Severe inflammation | Severe | Normal level of soft tissue | DAPI Collagen IV (488) CNA35(568) |

BCHI Bone Conduction Hearing Implant system. HA hydroxyapatite. DAPI 4′,6-Diamidino-2-Phenylindole, Dihydrochloride. CNA35 collagen-binding adhesion protein 35. Inflammation was measured using the Holger's Index [39] which was rescaled to a measure of inflammation: 0 – no, 1 – minor, 2 – moderate, 3–4 severe.

ments had been in situ for longer than one year. Three patients had a medical indication for the removal (Case 1, Case 2 and Case 4) and two patients were indicated for a change to a longer abutment (Case 3, Control 2). One unused HA-coated abutment (Control 3), taken directly from the sterile packaging, served as reference for HA autofluorescence.

### 3.2. Method validation using skin biopsies

Optimization and selection of staining protocols was achieved with skin biopsies (Control 1), as presented in Fig. 2. The cell nuclei (DAPI, blue) in the epidermal and dermal layer were clearly visualized (Fig. 2A–C). Nuclei of the keratinocytes appeared as a densely arranged cuboidal basal cell layer. The cells showed a flatter profile as they migrated towards the surface. Collagen IV of the basement membranes (green) and integrin-α6 staining of hemidesmosomes (red) are seen as mutually exclusive staining patterns at the dermal-epidermal junction (DEJ, Fig. 2A). Fig. 2B shows a skin appendage, where cells expressing a hemidesmosomal layer (integrin-α6, red) are enclosed by a thin basement membrane (collagen IV, green), again illustrating the mutual exclusiveness of the staining patterns. The second harmonic generated signal (SHG, cyan) of papillary dermal collagen shows a partial overlap with the collagen IV immunostaining pattern (Fig. 2A–B) as a result of their close proximity. The SHG signal was not as homogeneous and intense as that of the collagen staining by CNA35/AF568 (Fig. 2B–C). Therefore, the CNA35/AF568 was used as a collagen stain in the abutments.

### 3.3. All titanium abutment and unused reference HA-coated abutment

The surface of the titanium abutment (Control 2) did not show a significant amount of cell or tissue attachment as screened by using autofluorescence. No staining was performed. In Fig. 3A a characteristic image of a region with some amorphous material on the titanium surface is shown. The variance of the autofluorescent signal suggests that these patches of amorphous material consist of a combination of keratin, sebum, skin cells and bacteria, possibly in a biofilm.

The autofluorescence signal of the HA-coating of the unused reference abutment (Control 3) is presented in Fig. 3B. An overall signal was detected in a broad wavelength range, with the strongest signal appearing in the green channel (Fig. 3B). While the titanium surface was relatively smooth, as seen in Fig. 1A, the roughness of the HA-coating, as seen in Fig. 1B, was also observed with TPM (Fig. 3B).

### 3.4. Clinical cases

The demographics data and (immunofluorescent) staining methods of the four abutments that had been in situ for 1.5–2.5 years are summarized in Table 1.

*Case 1.* This abutment had been in situ for 2 years and was removed because of recurrent minor inflammation. It was stained for DNA (DAPI, blue), hemidesmosomes (integrin-α6, red) and collagen IV (green). Characteristic images are presented in Figs. 4 and 5. The reconstruction of all the stitched stacks produced the full-length abutment image in Fig. 4G, which shows the morphology of the tissue attached to the abutment. A clear gradient of increasing cellular density towards the bottom of the abutment is seen. The Ti-HA transition in Zone 1 showed presence of some clusters of cells in the cavities of the HA (Fig. 4A). Presence of structures indicative of neutrophil extracellular traps (NETs) could be identified by the presence of extracellular fibers of DNA [42] (Fig. 4B). Since the backbone of NETs is formed by DNA, common DNA stains can be used for their visualization [43,44]. However, no specific labeling for his-

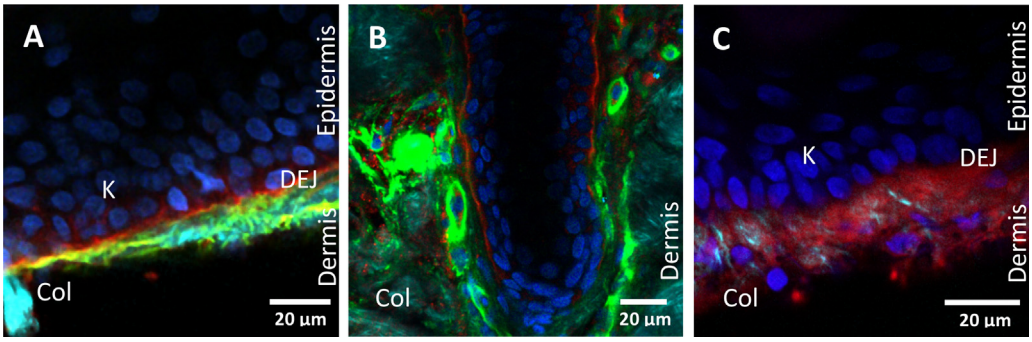


**Fig. 2.** Skin biopsies stained with the optimized protocol for validation purposes (Control 1).(For interpretation of the references to colour in this figure legend, the reader is referred to the web version of this article.)
**A)** Biopsy of full thickness retro-auricular skin stained for nuclei (DAPI, blue), collagen IV (green), and hemidesmosomes (integrin-α6, red). In the dermis, the second harmonic generated (SHG) signal (cyan) below the dermo-epidermal junction (DEJ) indicates the presence of collagen (Col). The DEJ is visible by the thin layer of hemidesmosomes (red, integrin-α6) above the layer of collagen IV (green), which is part of the basal lamina. The epidermis contains stratifying basal keratinocytes (K). **B)** Skin biopsy, stained for nuclei (blue), collagen IV (green), and integrin-α6 (red) showing staining of skin appendages. SHG signal from dermal collagen (Col) appears in cyan. **C)** Skin biopsy stained for nuclei with DAPI (blue) and dermal collagen (CNA35/AF568, red). The CNA35 and SHG signals overlap, but the CNA35 is more intense and more homogenous. Keratinocytes (K) densely and orderly arranged above the DEJ are visible.

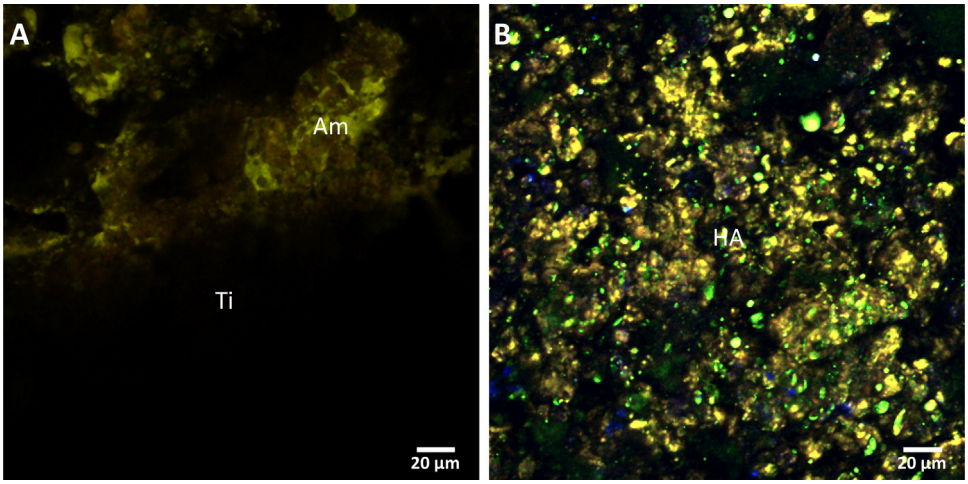


**Fig. 3.** Autofluorescence of a retrieved titanium abutment (Control 2) and unused HA-coated abutment (Control 3).
**A)** Titanium abutment (Ti) removed from a patient. A layer of amorphous materials (Am) with different autofluorescence signals was seen to a variable degree on top of the surface. There was no indication of structured tissue on top of the abutment. **B)** Hydroxyapatite (HA) coating of an unused abutment showing a distinct autofluorescence pattern with variability in structural composition of the granules.

tones or proteases has been used and therefore, although unlikely due to the mesh-like structure of the DNA, another source of this DNA (apoptotic cells, damaged nuclei etc.) cannot be excluded. In Zone 3, a layer of epithelial cells which seems to be attached to the HA is seen (Fig. 4C). The assumption that these are keratinocytes is based on the round morphology and typical dense packing [31]. The HA surface further down shows a faint immunostaining for integrin (red) in comparison to the region shown in Fig. 4c, which suggests hemidesmosomal attachment to the HA surface (Fig. 4D). We assume that these cells are basal keratinocytes (blue) as they express integrin-α6 (red) and are attached to the basement membrane, visualized by the presence of collagen IV (green). Zone 4, which corresponds to the concave part of the abutment, is covered with epithelial cells (Fig. 4E), where basal cells expressing integrin-α6 are attached to the HA coating. Near the lower end of the abutment (Fig. 4F), basal cells expressing integrin-α6 (red) and basement membrane containing collagen IV (green) are seen. A magnified region of Fig. 4F, showing the individual channels to highlight the presence and partial colocalization of collagen and integrins, is presented in Fig. 5. These results indicate that necessary components needed for integration of the skin with the abutment surface are present in each other's vicinity.

*Case 2.* This sample remained in situ for 2.5 years prior to removal due to ongoing severe inflammation. It was stained for nuclei (DAPI, blue) and fibrillar collagen (CNA35/OG488, green). Fig. 6A and B are taken from Zones 1 and 2, which both contained biofilm, and DNA structures strongly indicative for the presence of NETs. Cells were scarcely identified and exposed regions of HA were visible in this region. In Zones 3 and 4, numerous cells were visible and large surface areas were covered with biofilm (see Fig. 9), characterized by an intense autofluorescence [45] in combination with the DAPI signal (Fig. 6C). Cells (DAPI, blue) and biofilm in active dispersion (cyan) are visible in the center of the image, while no zones with dermal collagen were identified. In general, only a limited surface was covered by tissue from the host (see Fig. 9). Based on these results, the clinical diagnosis of infection was confirmed by the microscopic detection of biofilm. Furthermore, the presence of an extensive biofilm in this case is associated with the absence of indicators of integration.

*Case 3.* This sample was collected from a patient undergoing abutment replacement. The retrieved sample had remained in situ for 2 years and was removed due to skin overgrowth, which required a change to a longer abutment. No primary infection process was suspected for this sample. Upon removal, more force had

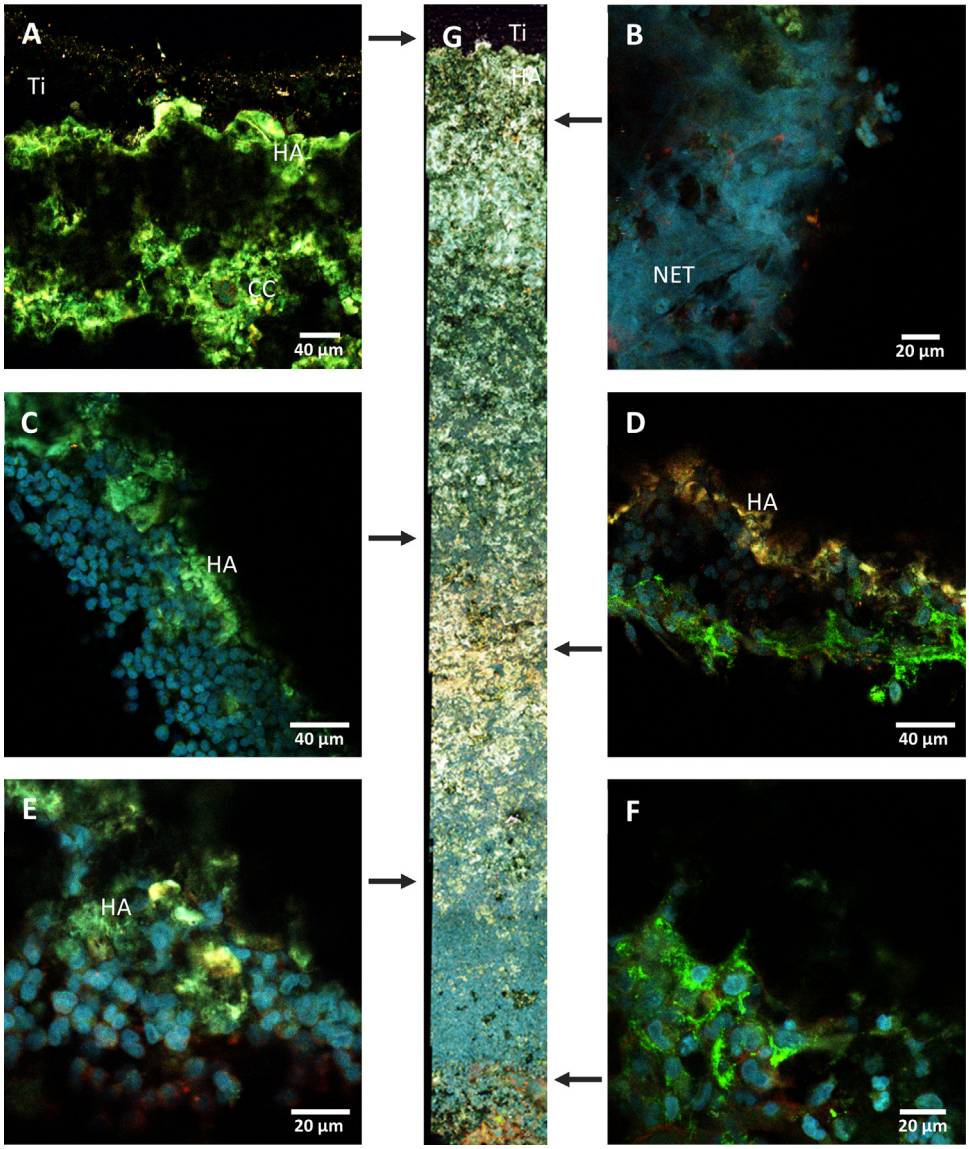


**Fig. 4.** Case 1–High resolution TPM images from Zones 1–4 and full-length abutment reconstruction.(For interpretation of the references to colour in this figure legend, the reader is referred to the web version of this article.)
The sample was stained for nuclei (DAPI, cyan), collagen IV (green) and hemidesmosomes (integrin-α6, red). **A)** Zone 1 of the abutment shows no cellular attachment to the titanium (Ti) and limited cellular attachment on the hydroxyapatite (HA, visualized by autofluorescence), usually in clusters of cells (CC). **B)** Extracellular DNA in the neighborhood of cells can be discerned (cyan) which could be interpreted as presence of neutrophil extracellular traps (NETs). **C)** Zone 3 with a layer of epithelial cells seeded onto the HA surface. **D)** Zone 3 with cells (cyan) near the surface expressing hemidesmosomes (red) and covered by collagen IV (green). **E)** Zone 4, cells (cyan) near the HA-surface expressing hemidesmosomes (red, integrin-α6). **F)** Cells (cyan) in Zone 4 expressing both Collagen IV (intense green) and hemidesmosomes (red). **G)** Maximum intensity projection along the full-length of the abutment surface. All images are in the XY plane (see Fig. 1C). Fig. 4A–F are single high resolution images acquired from regions depicted in the longitudinal stripe of Fig. 4G or adjacent regions. Arrows indicate the approximate level of Fig. 7A–F on the abutment.

to be applied to pull the abutment free from the bottom regions of the skin as compared to the other cases. The sample was stained for DNA (DAPI, blue), hemidesmosomes (integrin-α6, red) and collagen IV (green, and characteristic images are presented in Fig. 7. No epithelial cells are seen on the smooth titanium surface located above the Ti-HA transition (Zone 1, Fig. 7A), but instead amorphous material is attached. While the HA-coated part of the abutment in Zone 2 was abundantly covered by tissue, some regions showed exposed HA with clusters of cells within the cavities of the HA (Fig. 7B). Some of these cells express integrin-α6, typical of basal keratinocytes. The upper part of Zone 3 is characterized by clusters of cells expressing high levels of integrin-α6 (Fig. 7C), while cell clustering and expansion increases towards the lower part of Zone 3, completely covering the cavities of the HA coating. Zone 4 is densely occupied by epithelial cells, while several capillaries with a diameter ranging from 8 to 12 μm are visible between these cells (Fig. 7D). Fig. 7E shows a magnification of capillaries, where elongated endothelial cells, aligned with the vessel orientation, express integrin-α6 and are covered by a basement membrane containing collagen IV [46]. On this lower part of the abutment, connective tissue with sparsely arranged cells with an elongated nucleus, most likely fibroblasts, are seen (Fig. 7F). The faint green autofluorescence indicates the presence of dermal collagen in this region. These results indicate that in this case a high level of integration has been achieved. No signs of an extensive biofilm are observed.

*Case 4.* This sample remained in situ for 1.5 years, and was removed due to severe ongoing infection. Nuclei (DAPI, cyan), collagen IV (green) and dermal collagen (CNA35/AF568, red) were

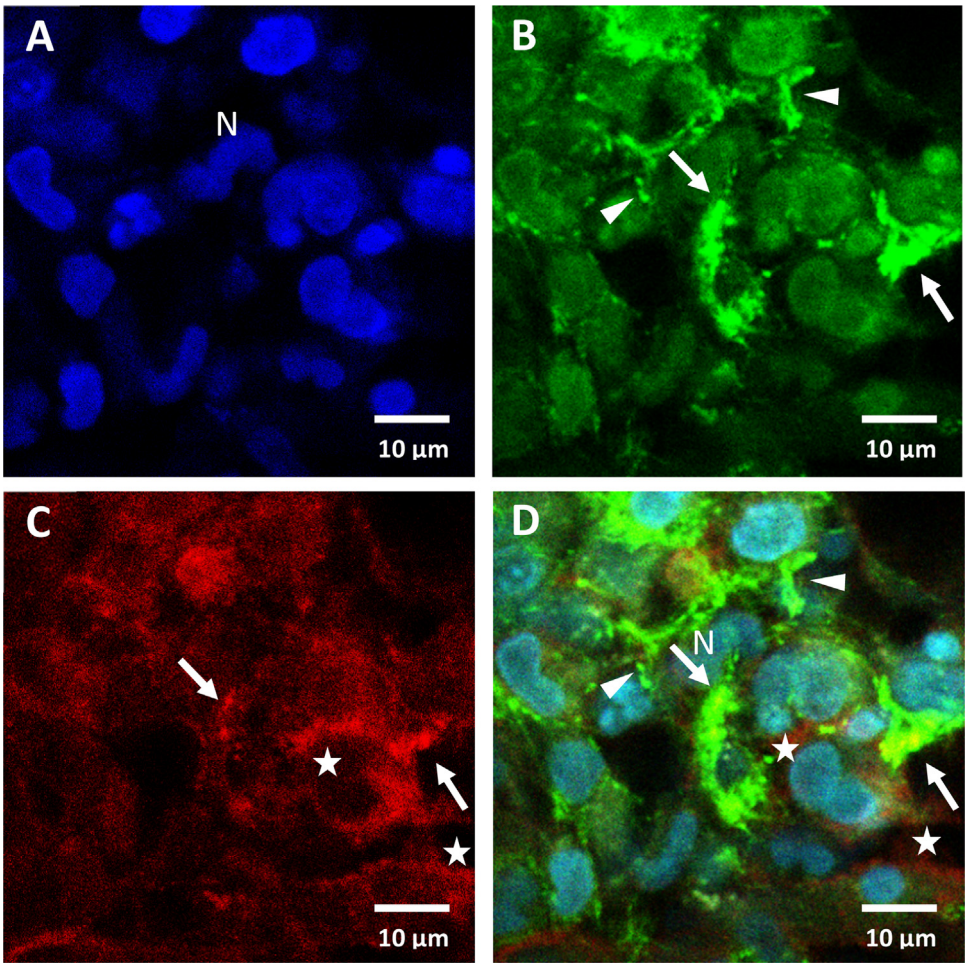


**Fig. 5. Case 1** Magnification and split channel images of Fig. 4F. **A)** Blue channel showing cell nuclei (N) stained with DAPI. **B)** Green channel showing collagen IV. **C)** Red channel showing integrin-α6. **D)** Merged channels. Arrowheads indicate collagen IV. Stars indicate integrin-α6. Arrows indicate integrin-α6 and collagen IV colocalization. (For interpretation of the references to colour in this figure legend, the reader is referred to the web version of this article.)

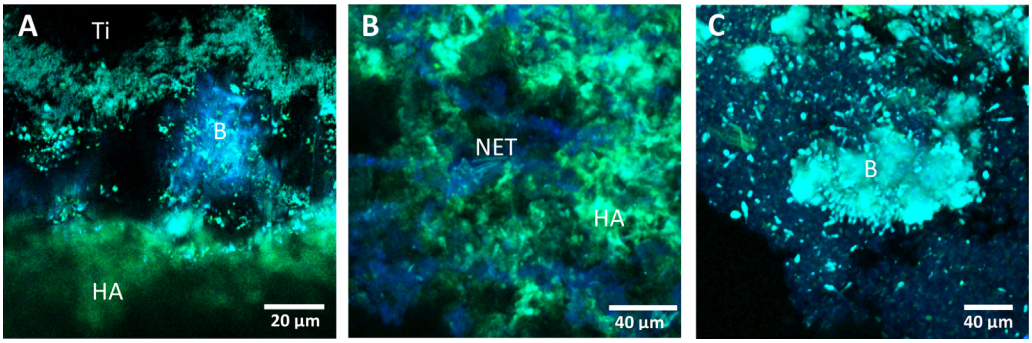


**Fig. 6. Case 2** Sample stained with DAPI (blue) showing extensive biofilm formation in all Zones. **A)** The transition from titanium to hydroxyapatite (HA) showing a plaque of biofilm (B) in Zone 1. **B)** Zone 2 showing bacteria in small colonies and DNA structures indicative of neutrophil extracellular traps (NETs) presence. **C)** Zone 3 with cells on top of the HA together with intensely fluorescent dispersing biofilm (B, cyan). (For interpretation of the references to colour in this figure legend, the reader is referred to the web version of this article.)

stained. On the titanium part of the abutment, in Zone 1, cells and NETs are visible together with depositions resembling stratum corneum (green) (Fig. 8A). Significant amounts of dermal collagen (red) were identified in Zone 2, together with cells (cyan) on top of HA (green), (Fig. 8B). Zone 3 was characterized by biofilm formation extending down to Zone 4 (see Fig. 9). The lower part of zone 4 (Fig. 8C) is occupied by a dense cellular layer. In this case a mixed state, featuring integration, inflammation and biofilm formation, can be discerned.

### *3.5. Full-length abutment surface reconstruction and case comparisons*

Fig. 9 displays the full-length abutment surface reconstructions of the four HA-coated abutments (Cases 1–4), while Fig. 10 displays the side view reconstructions of these cases. The images retain the high resolution of TPM while still allowing the full-length of the abutment to be visualized. Even though different stains were used in each case resulting in different color settings, cross comparison

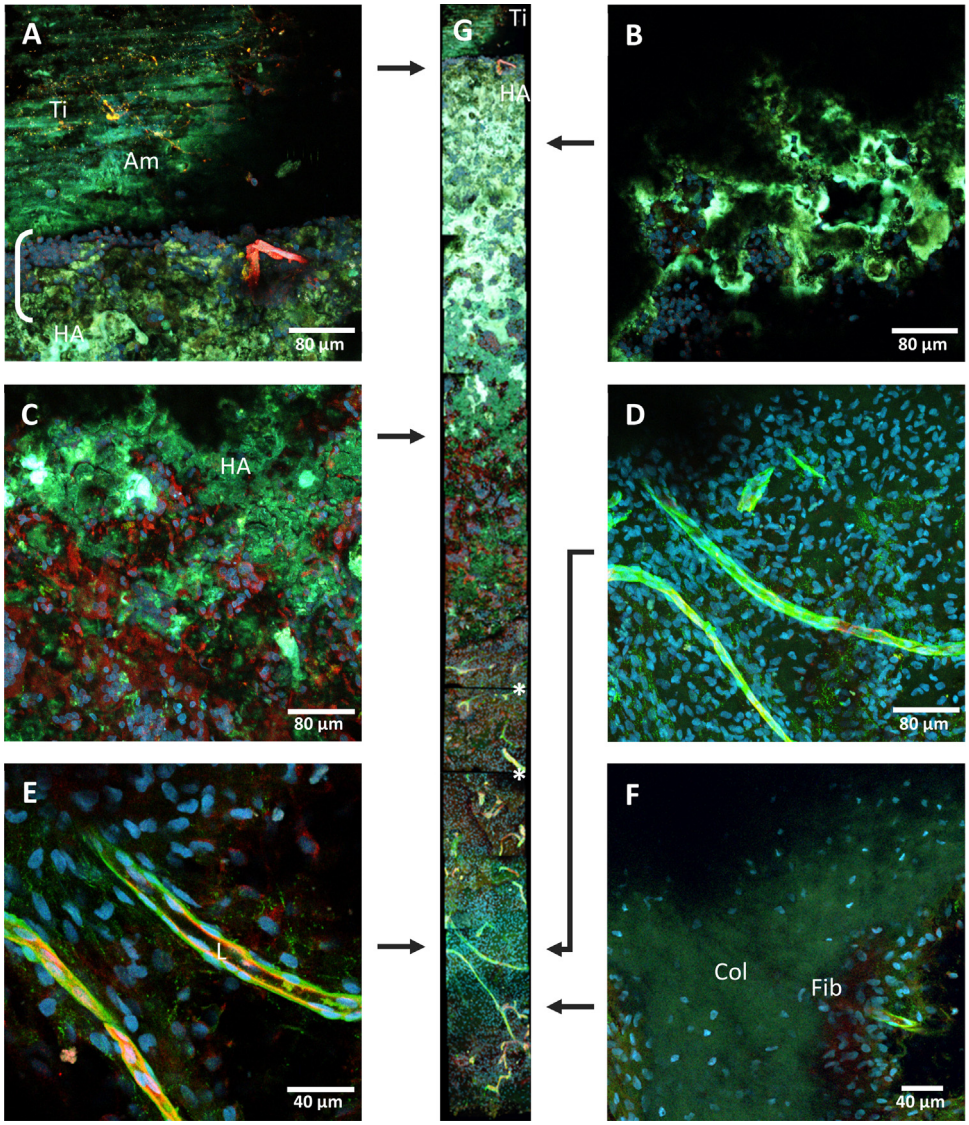


**Fig. 7.** Case 3–High resolution images from Zones 1–4 and full-length abutment reconstruction.(For interpretation of the references to colour in this figure legend, the reader is referred to the web version of this article.)
Sample stained for nuclei (DAPI), collagen IV, and hemidesmosomes (integrin-α6). **A)** Zone 1 of the abutment shows no cellular attachment to the titanium (Ti) but a green autofluorescent layer of amorphous material (Am) can be seen in this Ti region. On the hydroxyapatite (HA) region, however, cells (blue) are mostly present on the horizontal ridge (indicated with a bracket) of the Ti-HA transition. **B)** Cells (blue) in HA cavities (green) of Zone 2 showing absence or low expression of hemidesmosomal integrin-α6 (red). **C)** Cells (blue) on top of the HA (green) in Zone 3 with high expression levels of hemidesmosomal integrin-α6 (red). **D)** Capillaries as detected by collagen IV staining (green) and surrounded by cells (blue) are visible in Zone 4. **E)** A close up of the capillaries as shown in Fig. 7D. The endothelial cells surrounding the lumen (L) are recognized by the flattened nuclei (blue) and connect through hemidesmosomes (red) to the basement membrane (green) of the capillary. **F)** Zone 4 with sparsely arranged and elongated nuclei within a diffuse green autofluorescent background, which indicates the presence of dermal collagen (Col) with fibroblasts (Fib). **G)** Full-length abutment surface reconstruction. Discontinuities in the stitching and reconstruction process are indicated with an asterisk. All images are in the XY plane (see Fig. 1C) and except Fig. 7B are maximum intensity projections of a volume stack. Images 7A–7F are extracted from the longitudinal stripe presented in Fig. 7G. Arrows indicate the approximate level of Fig. 7A–F on the abutment.

is possible. Inspection of these four clinical cases revealed some common features. For Zone 1 around the Ti-HA transition, clusters of cells were mostly found on the HA side, continuing into Zone 2, while amorphous material was found on the titanium side. These amorphous materials were considered to be depositions of debris from stratum corneum and/or biofilm. In all cases, Zone 4 is densely populated by cells.

There is a clear distinction, however, between cases with and without severe inflammation. In the cases in which extensive biofilm is identified (cases 2 and 4), an immunological response is present (e.g. NETs). In both cases, only limited integration of the host tissue and the abutment surface could be observed. On the other hand, in cases 1 and 3, in which a limited amount or no biofilm is identified, a high level of skin integration is detected by expression of integrin-α6 and collagen IV. In addition, capillaries indicative of structural tissue organization, were identified in Case 3.

## 4. Discussion

The objective of this investigation was two-fold: first to develop and validate methods for imaging skin integration with abutments in clinical practice, and second to explore the modes of attachment of skin tissues to HA-coated abutments.

### 4.1. Imaging of skin integration

With respect to the first objective, the use of immunofluorescent markers in combination with TPM was shown to be effective

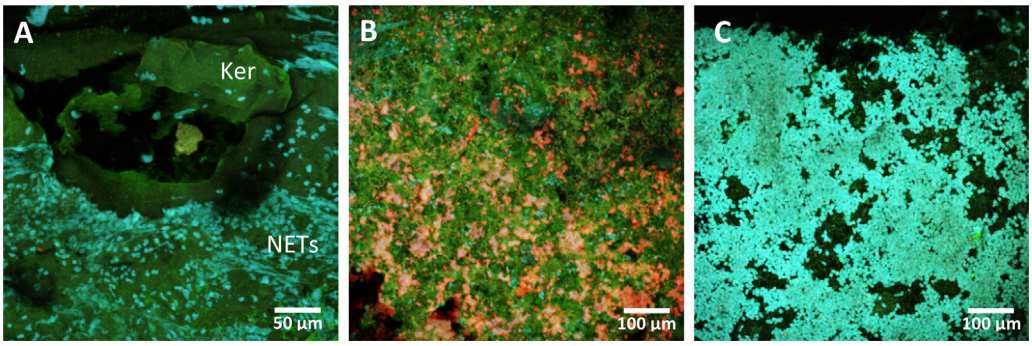


**Fig. 8. Case 4** Images showing staining of DNA (DAPI, cyan) and dermal collagen (CNA35, red). **A)** In Zone 1, on top of the titanium (Ti), neutrophil extracellular traps (NETs) (DAPI, cyan) are present together with biofilm and keratin depositions (Ker). **B)** Zone 2 contains cells (DAPI, cyan) scattered over the HA surface (green) and dermal collagen (red). **C)** Zone 4 contains tightly clustered cells. (For interpretation of the references to colour in this figure legend, the reader is referred to the web version of this article.)

in studying the tissues covering the HA-coated BCHI abutment surface. Immunofluorescence staining protocols using markers for skin integration, i.e. integrin-α6 and collagen IV, showing the known organization of hemidesmosomes and basement membranes on skin biopsies, gave valid results when applied to the tissues attaching to the retrieved abutments. Despite the thickness of the tissue attached to the abutment, staining was sufficiently homogeneous and the HA-coating could be visualized in most of the zones. Thus, the chosen method meets the requirements for ex vivo investigation of skin-abutment integration. The combination of TPM with the rotation mount allows imaging of any region of the abutment surface. In general, TPM is confined to a relatively small field of view (FOV). Imaging larger FOVs, i.e. in this investigation the entire length of the abutment, was made possible by stitching of adjacent images, replacing a need for conventional histological procedures [47]. In comparison to sample sectioning, this versatile three-dimensional imaging methodology provides a novel and more appropriate perspective of the tissue interacting with the abutment surface.

A qualitative assessment of the tissues attached to the abutments was performed. On the all-titanium control abutment no structural attachment of tissue was found, in line with previous investigations [48]. On all HA-coated abutments, however, tissue was found to be attached, but the amount of surface coverage varied. A gradual increase of tissue attachment was seen towards the concave zone, especially in the two cases with limited inflammation. This coincides with the finding of Larsson et al. that the shape of the abutment may influence tissue attachment [12]. Parts of the tissue that attached to the HA-coated surface showed evidence of hemidesmosomal adherence, indicative for the presence of basal keratinocytes. Collagen IV was present around cells on the surface of the HA-coating, which indicates the formation of a basement membrane. In one of the cases a high degree of tissue organization was achieved, with vascularization and dermal collagen extending over the surface of the abutment.

### 4.2. Modes of attachment

Previous animal studies [12,14], using conventional histological techniques on abutments left in situ for a short term (1 month), have suggested a mainly dermal type of adherence. The findings described above, however, support the hypothesis of a role for hemidesmosomes and basal lamina in skin integration with the HA-coating of abutments [13]. Therefore, an epidermal origin of the cells in the tissue attaching to the abutment is suggested. Also with respect to epidermal downgrowth differences were seen between these animal studies and our clinical observations. Epidermal downgrowth has been shown to be inhibited for the HA-coated abutment in comparison to the titanium control abutment in the short-term animal study [12,14]. In contrast, we observed epidermal downgrowth up to Zone 3. The specific phenotype and level of differentiation of the epithelial tissue of the epidermal downgrowth is different from the normal skin epidermis because it lacks cornification. Previously it was suggested that this tissue resembles junctional epithelium similar to that around teeth [13]. Since cornification, i.e. the presence of non-viable cells, is thought to inhibit integration, its absence may be beneficial. The skin-abutment interface shares many similarities with the enamel of the tooth-gingiva and maybe this system provides a model for a successful mode of attachment. In teeth, epithelial tissue in the junctional epithelium can attach through the internal basal lamina to the enamel of the tooth. Epithelial basal cells attach to the membrane through hemidesmosomes. Interestingly the enamel is constituted mainly of HA. However, in contrast to the internal basal lamina which is present in the skin, the internal basal lamina around teeth has no collagen IV. In the abutments extracted, we have observed a similar attachment mode, cells expressing hemidesmosomes are found on the interface of HA, but collagen IV has not always been identified in between this interface. This observation deserves further investigation by identifying molecules specific to internal basal lamina such as laminin 332 [49] to be labelled and verifying the presence or not of this internal basal lamina on this samples.

Additional to our findings of an epidermal attachment we also obtained indications for dermal attachment through collagen, which was observed either by means of autofluorescence or by direct collagen labeling with CNA35. Also, the presence of capillaries is suggestive for a dermal mode of attachment.

Since regions are observed where cells attaching to the abutment do not express collagen IV or integrin-α6, and where dermal collagen is absent, we hypothesize that a direct focal attachment might anchor these cells to the HA. These different modes of attachment may be simultaneously present around a single abutment.

### 4.3. Clinical associations

Several of the clinical observations can be supported by the microscopic findings. For example, the considerable pulling force required in Case 3 for the removal of the abutment from the skin is in line with the microscopically observed high level of integration.

Furthermore, the microscopic identification of biofilm, accompanied by NETs, could be associated with clinical signs of inflammation and infection. Most biofilm was present in areas where no structural attachment of tissue was seen. This mutual exclusiveness confirms the applicability of the "*race for the surface*" model.

Relevant factors for clinical outcomes in future investigations of skin integration include the degree of abutment surface tissue coverage, as well as prevention and healing of infections. The abil-

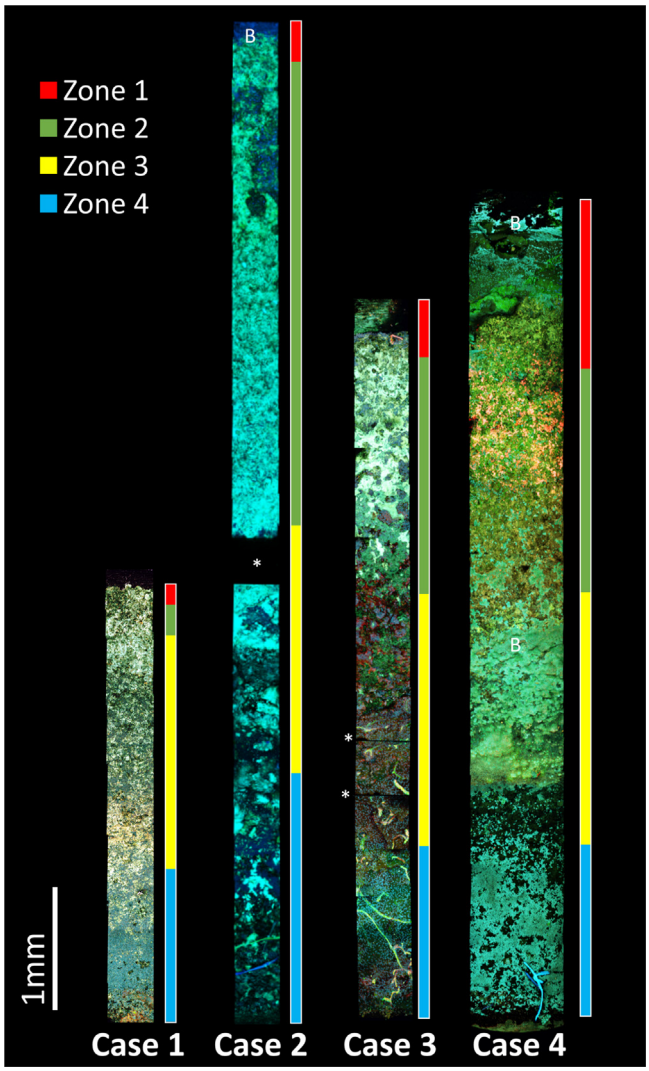


**Fig. 9.** Case comparisons of full-length abutment surface reconstruction.(For interpretation of the references to colour in this figure legend, the reader is referred to the web version of this article.)
The four cases have different abutment lengths (Table 1). In general, tissue attachment increased gradually from top to bottom. Tissue on the lower parts of the abutment in Case 3 showed vascularization in Zone 4. For the cases with peri-abutment dermatitis (Cases 2 and 4), extensive biofilm (B) was identified in several Zones. In these cases, cell attachment was less pronounced or even absent. For each case the microscopy settings had to be optimized for the individual fluorescence staining procedures, which did not allow for the direct color comparison. Discontinuities in the stitching and reconstruction process are indicated with an asterisk. The abutment zones are indicated with different colors seen on the legend on the top left.

ity of the skin-abutment interface to be repaired and maintained is important for the long term clinical stability and resilience. Our evidence of vascularization close to the abutment surface is an indication that the immune system has access to the abutment-skin interface, allowing prevention or clearing of infections.

We realize that by removing the abutment from the skin, the surrounding tissue is ruptured, which might result in an underestimation of the degree of skin integration. The relative strength of the connection between different tissue layers and between the tissue and the abutment surface will determine the location of the tissue rupture and, hence, the amount and nature of the tissue that remains on the abutment upon removal. Therefore, we have the opportunity to investigate the innermost tissue layers, which remained attached to the abutment surface when simply being unscrewed from the osseointegrating implant. Finally, it should be

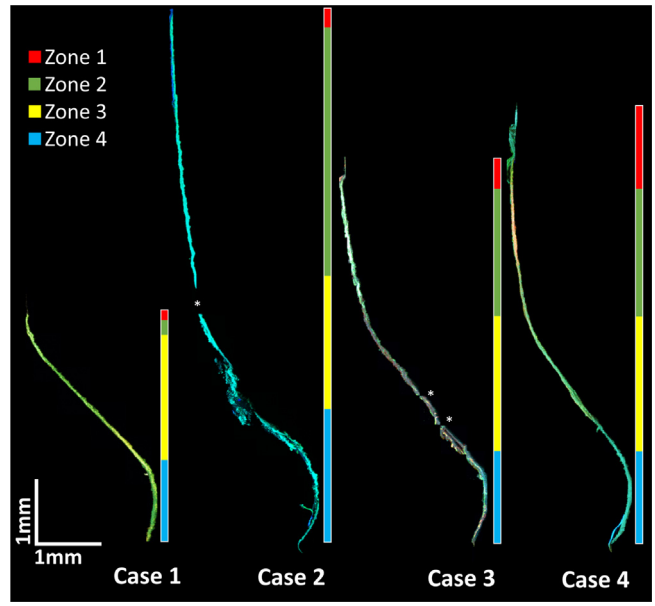


**Fig. 10.** Full-length abutment side view reconstructions.(For interpretation of the references to colour in this figure legend, the reader is referred to the web version of this article.)
Using a maximum intensity projection of the side view of the abutment surface, the thickness of the tissue attachment can be discerned. Discontinuities in the stitching and reconstruction process are indicated with an asterisk. The abutment zones are indicated with different colors seen on the legend on the top left.

kept in mind that the samples used in this study had a medical indication for removal. Therefore, the inflamed or infected samples are over-represented as compared to the clinical situation.

## 5. Conclusion

Investigating the attachment of tissue on abutment surfaces is possible and valid using two-photon microscopy. The methodology presented here allows for a high resolution and a large field of view, showing the entire length of the abutment, enabling ex vivo investigations into skin integration. Tissue attached to clinically retrieved HA-abutments expressed hemidesmosomes and collagen IV indicating skin integration. Findings in abutment samples with and without clinical signs of infection, showing the mutual exclusiveness of biofilm versus skin integration, support the *race for the surface model*.

## Acknowledgements

We acknowledge a research grant from Cochlear Bone Anchored Solutions AB, Mölnlycke, Sweden, which financially supported this investigator-initiated study. S. Wigren is a paid employee of Cochlear Bone Anchored Solutions AB. We gratefully acknowledge the kind gift of the collagen IV antibody by J. Cleutjens, Department of Pathology, Maastricht University Medical Centre and thank C. Reutelingsperger, Department of Biochemistry of Apoptosis, Maastricht University for labeling CNA35 with OG488 and AF568.

## References

[1] D. Campoccia, L. Montanaro, C.R. Arciola, A review of the biomaterials technologies for infection-resistant surfaces, Biomaterials 34 (2013) 8533–8554, http://dx.doi.org/10.1016/j.biomaterials.2013.07.089.
[2] H.J. Busscher, H.C. van der Mei, G. Subbiahdoss, P.C. Jutte, J.J. a M. van den Dungen, S. a J. Zaat, M.J. Schultz, D.W. Grainger, Biomaterial-associated infection: locating the finish line in the race for the surface, Sci. Transl. Med. 4 (2012), 153rv10, http://dx.doi.org/10.1126/scitranslmed.3004528.

[3] T.S. Kupper, R.C. Fuhlbrigge, Immune surveillance in the skin: mechanisms and clinical consequences, Nat. Rev. Immunol. 4 (2004) 211–222, http://dx.doi.org/10.1038/nri1310.
[4] F.O. Nestle, P. Di Meglio, J.-Z. Qin, B.J. Nickoloff, Skin immune sentinels in health and disease, Nat. Rev. Immunol. 9 (2009) 679–691, http://dx.doi.org/10.1038/nri2622.
[5] S. Franz, S. Rammelt, D. Scharnweber, J.C. Simon, Immune responses to implants – a review of the implications for the design of immunomodulatory biomaterials, Biomaterials 32 (2011) 6692–6709, http://dx.doi.org/10.1016/j.biomaterials.2011.05.078.
[6] J.M. Anderson, Biological responses to materials, Annu. Rev. Mater. 31 (2001) 81–110, http://dx.doi.org/10.1146/annurev.matsci.31.1.81.
[7] A. Tjellström, J. Lindström, O. Hallén, T. Albrektsson, P. Brånemark, Osseointegrated titanium implants in the temporal bone. A clinical study on bone-anchored hearing aids, Am. J. Otol. 2 (1981) 304–310.
[8] P.-I. Brånemark, U. Breine, R. Adell, B.O. Hansson, J. Lindström, Å. Ohlsson, Intra-osseous anchorage of dental Prostheses:I. Experimental studies, Scand. J. Plast. Reconstr. Surg. Hand Surg. 3 (1969) 81–100, http://dx.doi.org/10.3109/02844316909036699.
[9] A. Snik, E. Mylanus, D. Proops, J. Wolfaardt, W. Hodgetts, T. Somers, J. Niparko, J. Wazen, O. Sterkers, C. Cremers, A. Tjellström, Consensus statements on the BAHA system: where do we stand at present? Ann. Otol. Rhinol. Laryngol. Suppl. 195 (2005) 2–12.
[10] R.M. Strijbos, S.J.H. Bom, S. Zwerver, M.K.S. Hol, Percutaneous bone-anchored hearing implant surgery: dermatome versus linear incision technique, Eur. Arch. Oto-Rhino-Laryngol. 274 (2017) 109–117.
[11] M. Hultcrantz, Outcome of the bone-anchored hearing aid procedure without skin thinning: a prospective clinical trial, Otol. Neurotol. 32 (2011) 1134–1139.
[12] A. Larsson, S. Wigren, M. Andersson, G. Ekeroth, M. Flynn, U. Nannmark, Histologic evaluation of soft tissue integration of experimental abutments for bone anchored hearing implants using surgery without soft tissue reduction, Otol. Neurotol. 33 (2012) 1445–1451.
[13] M. van Hoof, S. Wigren, H. Duimel, P.H.M. Savelkoul, M. Flynn, R.J. Stokroos, Can the hydroxyapatite-coated skin-penetrating abutment for bone conduction hearing implants integrate with the surrounding skin? Front. Surg. 2 (2015) 45, http://dx.doi.org/10.3389/fsurg.2015.00045.
[14] A. Larsson, et al., Soft Tissue Integration of Hydroxyapatite-Coated Abutments for Bone Conduction Implants, Clin. Implant Dent. Relat. Res. 17 (Suppl 2) (2015) 730–735, http://dx.doi.org/10.1111/cid.12304.
[15] A. von Recum, Applications and failure modes of percutaneous devices: a review, J. Biomed. Mater. Res. 18 (1984) 323–623, http://dx.doi.org/10.1002/jbm.820180403.
[16] C. Pendegrass, D. Gordon, C. Middleton, S. Sun, G. Blunn, Sealing the skin barrier around transcutaneous implants: in vitro study of keratinocyte proliferation and adhesion in response to surface modifications of titanium alloy, J. Bone Joint Surg. Br. 90 (2008) 114–121.
[17] A. Gristina, Biomaterial-centered infection: microbial adhesion versus tissue integration, Science 237 (1987) 1588–1595.
[18] T. Bjarnsholt, M. Alhede, M. Alhede, S.R. Eickhardt-Sørensen, C. Moser, M. Kühl, Jensen P.Ø, N. Høiby, The in vivo biofilm, Trends Microbiol. 21 (2013) 466–474, http://dx.doi.org/10.1016/j.tim.2013.06.002.
[19] T. Bjarnsholt, K. Kirketerp-Møller, Jensen P.Ø, K.G. Madsen, R. Phipps, K. Krogfelt, N. Høiby, M. Givskov, Why chronic wounds will not heal: a novel hypothesis, Wound Repair Regen. 16 (2008) 2–10, http://dx.doi.org/10.1111/j.1524-475X.2007.00283.x.
[20] P.J. Sansonetti, J.P. Di Santo, Debugging how bacteria manipulate the immune response, Immunity 26 (2007) 149–161, http://dx.doi.org/10.1016/j.immuni.2007.02.004.
[21] C. Yue, B. Zhao, R. Kuijer, H.C. van der Mei, H.J. Busscher, E.T.J. Rochford, The implant infection paradox: why do some succeed when others fail? Opinion and discussion paper, Eur. Cells Mater. 29 (2015) 303–313, http://dx.doi.org/10.22203/eCM.v029a23.
[22] D. Davies, Understanding biofilm resistance to antibacterial agents, Nat. Rev. Drug Discov. 2 (2003) 114–122, http://dx.doi.org/10.1038/nrd1008.
[23] J. Anderson, A. Rodriguez, D. Chang, Foreign body reaction to biomaterials, Semin. Immunol. 20 (2008) 86–100.
[24] D. Baker, X. Liu, H. Weng, C. Luo, L. Tang, Fibroblast/fibrocyte: surface interaction dictates tissue reactions to micropillar implants, Biomacromolecules 12 (2011) 997–1005.
[25] G. Subbiahdoss, R. Kuijer, D. Grijpma, H. Mei, H. Busscher, Microbial biofilm growth vs. tissue integration: the race for the surface experimentally studied, Acta Biomater. 5 (2009) 1399–1404.
[26] R. Cicchi, D. Kapsokalyvas, V. De Giorgi, V. Maio, A. Van Wiechen, D. Massi, T. Lotti, F.S. Pavone, Scoring of collagen organization in healthy and diseased human dermis by multiphoton microscopy, J. Biophoton. 3 (2010) 34–43, http://dx.doi.org/10.1002/jbio.200910062.
[27] D. Kapsokalyvas, R. Cicchi, N. Bruscino, D. Alfieri, F. Prignano, D. Massi, T. Lotti, F.S. Pavone, In-vivo imaging of psoriatic lesions with polarization multispectral dermoscopy and multiphoton microscopy, Biomed. Opt. Express 5 (2014) 2405–2419, http://dx.doi.org/10.1364/BOE.5.002405.
[28] K. König, Clinical multiphoton tomography, J. Biophoton. 1 (2008) 13–23, http://dx.doi.org/10.1002/jbio.200710022.
[29] R. Cicchi, D. Kapsokalyvas, F.S. Pavone, Clinical nonlinear laser imaging of human skin: a review, Biomed. Res. Int. 2014 (2014), http://dx.doi.org/10.1155/2014/903589.
[30] R. Cicchi, D. Kapsokalyvas, M. Troiano, P. Campolmi, C. Morini, D. Massi, G. Cannarozzo, T. Lotti, F.S. Pavone, In vivo non-invasive monitoring of collagen remodelling by two-photon microscopy after micro-ablative fractional laser resurfacing, J. Biophoton. 7 (2013) 914–925, http://dx.doi.org/10.1002/jbio.201300124.
[31] D. Kapsokalyvas, R. Cicchi, N. Bruscino, D. Alfieri, F. Prignano, D. Massi, T. Lotti, F.S. Pavone, In-vivo imaging of psoriatic lesions with polarization multispectral dermoscopy and multiphoton microscopy, Biomed. Opt. Express 5 (2014) 2405–2419, http://dx.doi.org/10.1364/BOE.5.002405206234 (pii).
[32] J. Dowling, Q.C. Yu, E. Fuchs, Beta4 integrin is required for hemidesmosome formation, cell adhesion and cell survival, J. Cell Biol. 134 (1996) 559–572, http://dx.doi.org/10.1083/jcb.134.2.559.
[33] G. Walko, M.J. Castanon, G. Wiche, Molecular architecture and function of the hemidesmosome, Cell Tissue Res. 360 (2015) 363–378, http://dx.doi.org/10.1007/s00441-014-2061-z.
[34] M. Demarchez, D.J. Hartmann, M. Regnier, D. Asselineau, The role of fibroblasts in dermal vascularization and remodeling of reconstructed human skin after transplantation onto the nude mouse, Transplantation 54 (1992) 317–326, http://dx.doi.org/10.1097/00007890-199208000-00023.
[35] H. Hasegawa, I. Naito, K. Nakano, R. Momota, K. Nishida, T. Taguchi, Y. Sado, Y. Ninomiya, A. Ohtsuka, The distributions of type IV collagen alpha chains in basement membranes of human epidermis and skin appendages, Arch. Histol. Cytol. 70 (2007) 255–265 (JST.JSTAGE/aohc/70.255 [pii]).
[36] K.N. Krahn, C.V.C. Bouten, S. Van Tuijl, M.A.M.J. Van Zandvoort, M. Merkx, Fluorescently labeled collagen binding proteins allow specific visualization of collagen in tissues and live cell culture, Anal. Biochem. 350 (2006) 177–185, http://dx.doi.org/10.1016/j.ab.2006.01.013.
[37] R.T. Megens, M.G. Oude Egbrink, J.P. Cleutjens, M.J. Kuijpers, P.H. Schiffers, M. Merkx, D.W. Slaaf, M.A. van Zandvoort, Imaging collagen in intact viable healthy and atherosclerotic arteries using fluorescently labeled CNA35 and two-photon laser scanning microscopy, Mol. Imaging 6 (2007) 247–260 http://www.ncbi.nlm.nih.gov/entrez/query.fcgi?cmd=Retrieve&db=PubMed&dopt=Citation&list_uids=17711780.
[38] M.G. Havenith, J.P.M. Cleutjens, C. Beek, E. v d Linden, A.F.P.M. De Goeij, F.T. Bosman, Human specific anti-type IV collagen monoclonal antibodies, characterization and immunohistochemical application, Histochemistry 87 (1987) 123–128.
[39] K.M. Holgers, A. Tjellström, L.M. Bjursten, B.E. Erlandsson, Soft tissue reactions around percutaneous implants: a clinical study of soft tissue conditions around skin-penetrating titanium implants for bone-anchored hearing aids, Am. J. Otol. 9 (1988) 56–59.
[40] S. Preibisch, S. Saalfeld, P. Tomancak, Globally optimal stitching of tiled 3D microscopic image acquisitions, Bioinformatics 25 (2009) 1463–1465, http://dx.doi.org/10.1093/bioinformatics/btp184.
[41] J. Schindelin, I. Arganda-Carreras, E. Frise, V. Kaynig, M. Longair, T. Pietzsch, S. Preibisch, C. Rueden, S. Saalfeld, B. Schmid, J.Y. Tinevez, D.J. White, V. Hartenstein, K. Eliceiri, P. Tomancak, A. Cardona, Fiji: an open-source platform for biological-image analysis, Nat. Methods 9 (2012) 676–682, http://dx.doi.org/10.1038/Nmeth.2019.
[42] V. Brinkmann, U. Reichard, C. Goosmann, B. Fauler, Y. Uhlemann, D.S. Weiss, Y. Weinrauch, A. Zychlinsky, Neutrophil extracellular traps kill bacteria, Science 20 (303) (2004) 1532–1535, http://dx.doi.org/10.1126/science.1092385.
[43] S. Masuda, D. Nakazawa, H. Shida, A. Miyoshi, Y. Kusunoki, U. Tomaru, A. Ishizu, NETosis markers: quest for specific, objective, and quantitative markers, Clin. Chim. Acta 459 (2016) 89–93, http://dx.doi.org/10.1016/j.cca.2016.05.029.
[44] T. Saitoh, J. Komano, Y. Saitoh, T. Misawa, M. Takahama, T. Kozaki, T. Uehata, H. Iwasaki, H. Omori, S. Yamaoka, N. Yamamoto, S. Akira, Neutrophil extracellular traps mediate a host defense response to human immunodeficiency virus-1, Cell Host Microbe 12 (2012) 109–116, http://dx.doi.org/10.1016/j.chom.2012.05.015.
[45] L. Yang, Y. Zhou, S. Zhu, T. Huang, L. Wu, X. Yan, Detection and quantification of bacterial autofluorescence at the single-cell level by a laboratory-built high-sensitivity flow cytometer, Anal. Chem. 84 (2012) 1526–1532, http://dx.doi.org/10.1021/ac2031332.
[46] L. Primo, G. Seano, C. Roca, F. Maione, P.A. Gagliardi, R. Sessa, M. Martinelli, E. Giraudo, L. di Blasio, F. Bussolino, Increased expression of α6 integrin in endothelial cells unveils a proangiogenic role for basement membrane, Cancer Res. 70 (2010) 5759–5769.
[47] M.D. Rohrer, C.C. Schubert, The cutting-grinding technique for histologic preparation of undecalcified bone and bone-anchored implants. Improvements in instrumentation and procedures, Oral Surgery, Oral Med. Oral Pathol. 74 (1992) 73–78, http://dx.doi.org/10.1016/0030-4220(92)90218-F.
[48] K. Holgers, P. Thomsen, A. Tjellström, L. Ericson, Electron microscopic observations on the soft tissue around clinical long-term percutaneous titanium implants, Biomaterials 16 (1995) 83–90.
[49] H. Larjava, L. Koivisto, L. Hakkinen, J. Heino, Epithelial integrins with special reference to oral epithelia, J. Dent. Res. 90 (2011) 1367–1376, http://dx.doi.org/10.1177/0022034511402207.